JCI The Journal of Clinical Investigation

Heparan sulfate mimetic PG545-mediated antilymphoma effects require TLR9-dependent NK cell activation

Todd V. Brennan, … , Xiaopei Huang, Yiping Yang

J Clin Invest. 2016;126(1):207-219. https://doi.org/10.1172/JCI76566.

Research Article **Oncology**

Heparan sulfate (HS) is an essential component of the extracellular matrix (ECM), which serves as a barrier to tumor invasion and metastasis. Heparanase promotes tumor growth by cleaving HS chains of proteoglycan and releasing HS-bound angiogenic growth factors and facilitates tumor invasion and metastasis by degrading the ECM. HS mimetics, such as PG545, have been developed as antitumor agents and are designed to suppress angiogenesis and metastasis by inhibiting heparanase and competing for the HS-binding domain of angiogenic growth factors. However, how PG545 exerts its antitumor effect remains incompletely defined. Here, using murine models of lymphoma, we determined that the antitumor effects of PG545 are critically dependent on NK cell activation and that NK cell activation by PG545 requires TLR9. We demonstrate that PG545 does not activate TLR9 directly but instead enhances TLR9 activation through the elevation of the TLR9 ligand CpG in DCs. Specifically, PG545 treatment resulted in CpG accumulation in the lysosomal compartment of DCs, leading to enhanced production of IL-12, which is essential for PG545-mediated NK cell activation. Overall, these results reveal that PG545 activates NK cells and that this activation is critical for the antitumor effect of PG545. Moreover, our findings may have important implications for improving NK cell–based antitumor therapies.

Heparan sulfate mimetic PG545-mediated antilymphoma effects require TLR9-dependent NK cell activation

Todd V. Brennan,[1] Liwen Lin,[1] Joshua D. Brandstadter,[2] Victoria R. Rendell,[1] Keith Dredge,[3] Xiaopei Huang,[2] and Yiping Yang[2,4]

[1]Department of Surgery and [2]Department of Medicine, Duke University Medical Center, Durham, North Carolina, USA. [3]Progen Pharmaceuticals Limited, Darra, Queensland, Australia. [4]Department of Immunology, Duke University Medical Center, Durham, North Carolina, USA.

Heparan sulfate (HS) is an essential component of the extracellular matrix (ECM), which serves as a barrier to tumor invasion and metastasis. Heparanase promotes tumor growth by cleaving HS chains of proteoglycan and releasing HS-bound angiogenic growth factors and facilitates tumor invasion and metastasis by degrading the ECM. HS mimetics, such as PG545, have been developed as antitumor agents and are designed to suppress angiogenesis and metastasis by inhibiting heparanase and competing for the HS-binding domain of angiogenic growth factors. However, how PG545 exerts its antitumor effect remains incompletely defined. Here, using murine models of lymphoma, we determined that the antitumor effects of PG545 are critically dependent on NK cell activation and that NK cell activation by PG545 requires TLR9. We demonstrate that PG545 does not activate TLR9 directly but instead enhances TLR9 activation through the elevation of the TLR9 ligand CpG in DCs. Specifically, PG545 treatment resulted in CpG accumulation in the lysosomal compartment of DCs, leading to enhanced production of IL-12, which is essential for PG545-mediated NK cell activation. Overall, these results reveal that PG545 activates NK cells and that this activation is critical for the antitumor effect of PG545. Moreover, our findings may have important implications for improving NK cell–based antitumor therapies.

Introduction

The extracellular matrix (ECM) is composed of an interlocking mesh of proteins, proteoglycans, and glycosaminoglycans (GAGs) that are critical mediators of tumor growth and metastasis. The ECM not only provides structure for tumor growth, but also acts as a barrier to tumor metastasis. Heparan sulfate (HS), a GAG found abundantly in the ECM of most tissues, is a highly sulfated polysaccharide and has been shown to regulate several aspects of cancer biology, including angiogenesis, tumor progression, and metastasis (1–4).

Heparanase is the sole mammalian endoglucuronidase that cleaves side chains of HS proteoglycan. Preferential expression of heparanase has been found in various types of cancer, and patients with cancer with high expression levels are considered to have a poor prognosis (5–9). Heparanase degradation of the ECM not only facilitates intercellular tumor invasion and metastasis via disassembly of extracellular barriers, but also releases HS-bound angiogenic growth factors, such as VEGF, FGF-1, and FGF-2, from the ECM (reviewed in ref. 3). Their association with HS promotes growth factor receptor binding and signaling. In addition, HS released by heparanase is a potent endogenous TLR4 agonist that can provide pro-oncogenic signals through the downstream activation of NF-κB through phosphorylated activation of ERK1/2 and p38 (10, 11).

Given the important role of heparanase and HS in cancer progression, HS mimetics that inhibit heparanase and compete for the HS-binding domain of angiogenic growth factors have been developed as novel antitumor agents (12, 13). Indeed, HS mimetics have demonstrated antitumor activities in multiple preclinical studies of metastatic solid tumors in mice (14–17). Moreover, a number of HS mimetics are currently under clinical investigation for various cancers — muparfostat in hepatitis virus–related hepatocellular carcinoma after surgical resection, roneparstat in multiple myeloma, and necuparanib in pancreatic cancer. In contrast to these agents, PG545 is a single molecular entity, a synthetically manufactured tetrasaccharide with a lipophilic modification. This design not only enhanced antitumor and antimetastatic activity, but also significantly increased in vivo half-life compared with typical HS mimetics (13, 14, 16, 18). In addition, PG545 exhibits very mild anticoagulant activity, a common side effect of HS mimetics (19–21). A phase I trial of PG545 is ongoing in patients with advanced cancer (ClinicalTrials.gov NCT02042781).

Although the conventional antitumor mechanism for HS mimetics is the inhibition of angiogenesis and metastasis (13, 14, 16, 22, 23), HS and heparanase have been associated with inflammatory responses (12, 24, 25) and the effects of PG545 on immune cells have not been specifically investigated. In this study, we found that PG545 had potent antitumor activity in murine models of B cell and T cell lymphomas. Investigation into the mechanism revealed that the in vivo antitumor effect of PG545 was depen-

Note regarding evaluation of this manuscript: Manuscripts authored by scientists associated with Duke University, The University of North Carolina at Chapel Hill, Duke-NUS, and the Sanford-Burnham Medical Research Institute are handled not by members of the editorial board but rather by the science editors, who consult with selected external editors and reviewers.

Conflict of interest: Keith Dredge is an employee of Progen Pharmaceuticals Limited.

Submitted: March 25, 2015; **Accepted:** November 3, 2015.

Reference information: *J Clin Invest*. 2016;126(1):207–219. doi:10.1172/JCI76566.

dent on the activation of NK cells and that NK cell activation by PG545 was mediated through the TLR9/MyD88 pathway in vivo. We next showed that PG545 substantially enhanced CpG-mediated activation of TLR9 on DCs in vitro. This was accomplished by promoting the accumulation of CpG in the lysosomal compartment of DCs, leading to enhanced production of IL-12. We further demonstrated that TLR9-dependent production of IL-12 was critical for PG545-mediated NK cell activation in vivo. Collectively, these findings reveal what we believe to be a novel function for the HS mimetic, PG545, in activating NK cells, which is critical for the antitumor effect of PG545 in vivo.

Results

PG545 possesses antilymphoma activity in mice. To determine whether PG545 possesses antitumor activity against hematological malignancies, we first used an in vivo model of A20 B cell lymphoma (derived from BALB/c mice). In order to quantify overall tumor burden in vivo, an A20 lymphoma cell line stably expressing firefly luciferase was generated (referred to herein as the A20-luciferase cell line) by lentiviral transduction and single-cell cloning. BALB/c mice were injected with 2×10^5 A20-luciferase cells intravenously 1 day following PG545 treatment. Mice were then treated with PG545 once weekly, and tumor growth was monitored by measuring luciferase activity. We found that A20 lymphoma grew rapidly in PBS-treated (control) mice and that all mice succumbed to tumor growth within 55 days of tumor transfer (Figure 1, A–C). However, once-weekly injection of PG545 suppressed tumor growth and significantly prolonged survival (Figure 1, A–C).

To investigate whether PG545 is effective against a different lymphoma on a different genetic background, we performed similar experiments using a model of EL-4 T cell lymphoma (derived from C57BL/6 mice). C57BL/6 mice were inoculated with 1×10^5 EL-4-luciferase lymphoma cells subcutaneously and given weekly PG545 treatments, beginning the day of tumor inoculation. Again, we observed that PG545 was effective in preventing the growth of EL-4 T cell lymphoma and significantly prolonged survival (Figure 1, D–F). Thus, we concluded that PG545 could suppress the growth of both B cell and T cell lymphomas in vivo.

To determine whether PG545 is capable of treating preestablished lymphoma, mice were first inoculated with A20-luciferase cells intravenously. One and three days later, mice were treated with PG545 once weekly, and tumor growth and survival were monitored. We found that PG545 treatment significantly delayed tumor growth (Figure 2A) and prolonged survival (Figure 2B) in comparison to those in the vehicle-treated (PBS-treated) controls, suggesting that PG545 is also effective in treating preestablished lymphoma.

To more vigorously test whether PG545 can treat preestablished large tumor burden, mice were first intravenously injected with A20-luciferase cells, and in vivo luciferase imaging was used to follow tumor development. Once tumors were detectable at greater than 10^5 photons emitted per second, which occurred at between 3 and 4 weeks after tumor injection on average, mice received treatment with low-dose cyclophosphamide (CP) alone (50 mg/kg, i.p., single injection), PG545 alone (20 mg/kg, s.c., weekly injections), CP and PG545 combined therapy, or PBS (vehicle) only. While low-dose CP resulted in a brief decrease in tumor burden, there was a rapid regrowth of the tumors in the majority of mice, with growth kinetics similar to those in the PBS-treated group (Figure 2C). In comparison, the PG545-treated cohort demonstrated complete tumor remission, as shown by the return of luminescence to baseline (no tumor) levels (Figure 2C) and tumor-free survival at 60 days from the initiation of treatment (Figure 2D).

Antilymphoma activity of PG545 is dependent on activation of NK cells in vivo. How does PG545 exert an antitumor effect in vivo? Given the role of HS and heparanase in the inflammatory response (12, 24, 25) and their association with cells of the immune system (10, 11), we examined whether PG545 could activate immune cells, such as T and NK cells. BALB/c mice were treated with either PG545 or PBS, and NK and T cells were analyzed 2 days later by FACS. We observed that in comparison to that in the PBS control group, treatment with PG545 promoted NK cell activation, proliferation, and function, as shown by the upregulation of CD69, Ki-67, and IFN-γ expression, respectively (Figure 3, A and B). In comparison, PG545 resulted in minimal T cell upregulation of CD69 and no significant increase in T cell CD69, Ki-67, or IFN-γ expression (Figure 3, A and C). Furthermore, PG545 caused an expansion of NK cells in vivo, peaking with nearly a 10-fold increase in splenic NK cells 5 days following a single subcutaneous injection of PG545, compared with that after injection with PBS (vehicle) alone (Figure 3D). In addition, PG545-activated NK cells demonstrated increased cytotoxic function against Yac-1 target cells, as compared with NK cells from mice injected with PBS or polyinosinic-polycytidylic acid [Poly(I:C)] (Figure 3E). In addition, compared with commonly used NK activators, CpG oligodeoxynucleotides (ODNs), and Poly(I:C), PG545 produced higher levels of CD69, Ki-67, and IFN-γ expression in NK cells in vivo (Supplemental Figure 1; supplemental material available online with this article; doi:10.1172/JCI76566DS1). These results indicated that administration of PG545 promotes NK cell activation, expansion, and cytotoxicity.

We next assessed the NK cell and T cell responses to PG545 in tumor-bearing mice over time. Mice were intravenously injected with A20-luciferase cells. Three to four weeks after tumor injection, mice received treatment with low-dose CP alone (50 mg/kg, i.p., single injection), PG545 alone (20 mg/kg, s.c., weekly injections), CP and PG545 combined therapy, or PBS (vehicle) only. Mice from each treatment group were then sacrificed at 2, 5, 13, and 20 days from the start of treatment (Supplemental Figure 2). PG545 was administered on days 0, 7, and 14, such that mice harvested on days 13 and 20 were representative of trough PG545 levels. Splenic NK cells were then quantified and analyzed for function in terms of IFN-γ production and CD107a mobilization. As shown in Supplemental Figure 2, both the PG545 treatment only and the CP and PG545 combined therapy groups demonstrated greater NK expansion, IFN-γ production, and CD107a mobilization compared with those in the CP alone or PBS (vehicle) treatment groups. Interestingly, the NK activation persisted throughout the course of therapy, and T cells did not demonstrate any increase in these markers of activation. Next, we performed immunohistochemistry on liver sections with lymphoma to access the localization of NK cells within tumors. Compared

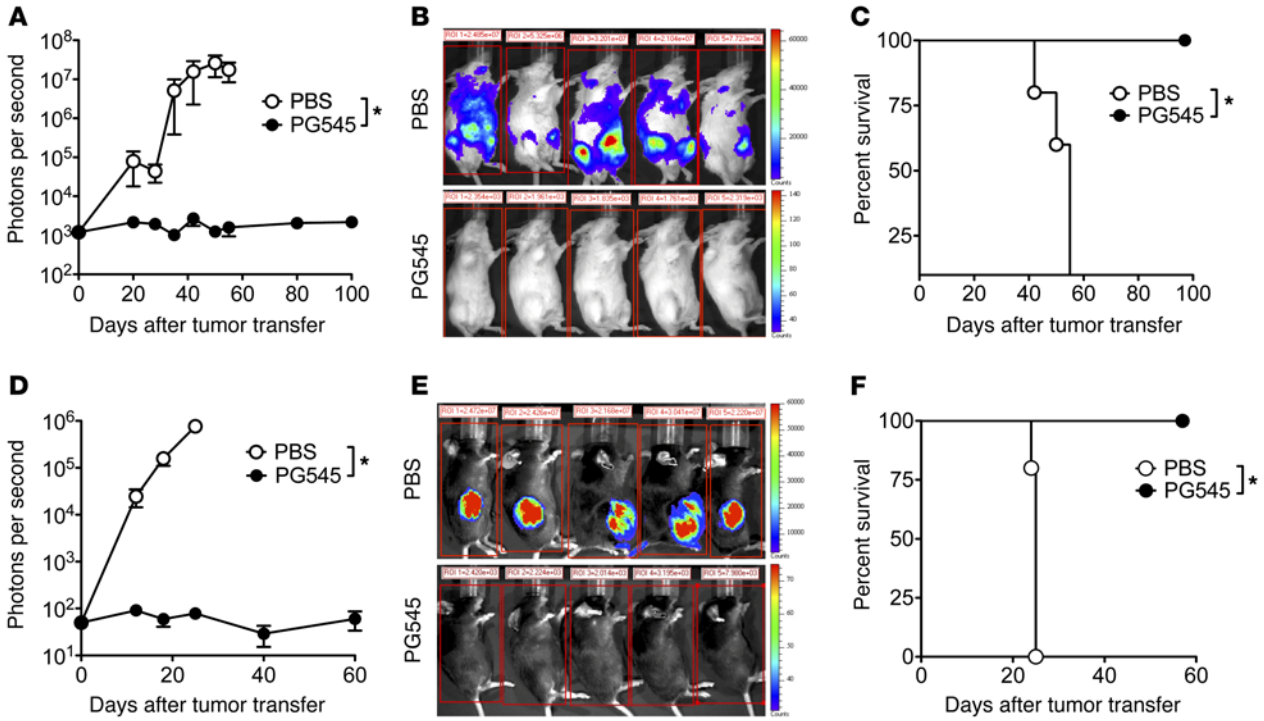

Figure 1. PG545 suppresses tumor development in murine models of lymphoma. (**A**–**C**) BALB/c mice were injected intravenously with 2×10^5 luciferase-expressing A20 (B cell lymphoma) cells and (**D**–**F**) C57BL/6 mice were injected subcutaneously with 1×10^5 luciferase-expressing EL-4 (T cell lymphoma) cells. Mice were then treated with either once-weekly injection of PG545 (20 mg/kg, s.c.) or vehicle alone (PBS), beginning 1 day prior to tumor inoculation. (**A** and **D**) Tumor burden was quantified over time as photons per second following D-luciferin injection. Examples of in vivo luciferase imaging are shown for (**B**) day 35 after injection of A20 and (**E**) day 20 following injection of EL-4. Survival of mice with (**C**) A20 or (**F**) EL-4 tumors was compared between PG545-treated and PBS-treated mice by Kaplan-Meier survival analysis. $n = 5$ per group. Results representative of 2 independent experiments. $^*P < 0.05$, Kruskal-Wallis test (**A** and **D**); log-rank test (**C** and **F**).

with tumors in CP- or PBS-treated mice, tumors in PG545-treated mice had more abundant NK cells within the tumor. Mice in the CP and PG545 combined therapy group had no tumors to access.

We next determined whether NK cells were necessary for the PG545-dependent antitumor effect. To address this question, we examined the effect of NK depletion on the antitumor effect of PG545. BALB/c mice were first depleted of NK cells by twice-weekly injections of anti-asialo GM1 antibody (Supplemental Figure 3, A and B) and then challenged with A20-luciferase lymphoma, along with either PB545 treatment or vehicle alone (PBS). We found that depletion of NK cells abolished the antitumor activity of PG545, leading to rapid tumor growth and mortality (Figure 4, A and B). To investigate whether NK cells were essential for PG545 function against a different lymphoma on a different genetic background, we first depleted C57BL/6 mice with anti-NK1.1 antibody (Supplemental Figure 3, C and D) and then challenged them with EL-4-luciferase lymphoma, along with either PB545 treatment or vehicle alone (PBS). Again, we found that depletion of NK cells abolished the antitumor activity of PG545, leading to rapid tumor growth and mortality (Figure 4, C and D). These results indicated that NK cells are critical to the in vivo antitumor effect of PG545.

Activation of NK cells by PG545 is mediated through the TLR9/MyD88 pathway. We next investigated the mechanism by which PG545 activates NK cells. Studies have shown that TLR pathways of the innate immune system play an important role in NK cell activation and function (26). Since HS has been shown to be an endogenous TLR4 ligand (11, 27), we first tested whether PG545, a HS mimetic, could also serve as a TLR4 agonist to activate NK cells through the TLR4 pathway. To address this question, mice deficient for TLR4 (*Tlr4*$^{-/-}$) were treated with PG545 and examined for NK cell activation, proliferation, and function by FACS 2 days later. Interestingly, we found no difference in PG545-induced expression of CD69, Ki-67, and IFN-γ by NK cells in *Tlr4*$^{-/-}$ mice and WT mice (Figure 5), suggesting that TLR4 is not involved in PG545-dependent NK cell activation. Instead, we observed that *Tlr9*$^{-/-}$ mice demonstrated a complete absence of NK cell activation in response to PG545 treatment (Figure 5). These results indicated that TLR9 was necessary for the activation of NK cells by PG545.

Studies have shown that MyD88 is a common adaptor for intracellular signaling of all TLRs except TLR3, which is mediated by TRIF (28, 29). Consistent with the TLR9 dependence of PG545, we further found that MyD88, but not TRIF, was critical for PG545-dependent NK cell activation (Figure 5). Collectively, our results indicate that the activation of NK cells by PG545 is mediated through the TLR9/MyD88 pathway.

PG545 enhances CpG-mediated activation of TLR9. The dependency of PG545-mediated NK cell activation on the TLR9 pathway suggested that PG545 could activate TLR9 either directly or indirectly by promoting TLR9 activation through its ligand, CpG.

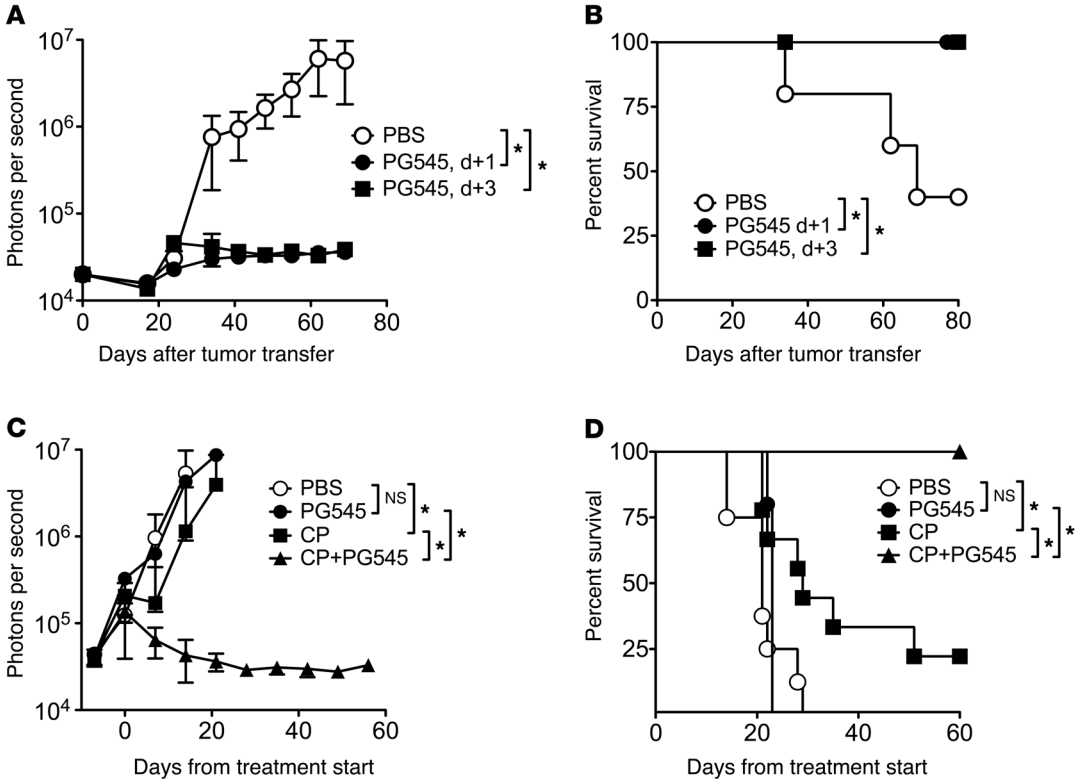

Figure 2. PG545 is effective in an established lymphoma model. (**A** and **B**) BALB/c mice were injected intravenously with 2×10^5 luciferase-expressing A20 cells and received once-weekly PG545 (20 mg/kg, s.c.) beginning day 1 (d+1) or day 3 (d+3) following tumor inoculation. (**A**) Tumor burden was quantified over time by IVIS, and (**B**) survival of mice with A20 tumors was compared between PG545-treated and PBS-treated mice by Kaplan-Meier survival analysis. $n = 5$ per group. $^*P < 0.05$. (**C** and **D**) BALB/c mice were injected intravenously with 2×10^5 luciferase-expressing A20 cells, and tumor growth was followed by IVIS until total body tumor burden produced 10^5 photons per second. Mice were then treated with CP alone (50 mg/kg, i.p., single dose), PG545 (20 mg/kg, s.c., once-weekly dosing), CP plus PG545, or PBS (vehicle). (**C**) Tumor burden was quantified over time by IVIS, and (**D**) survival of mice with A20 tumors was compared between groups by Kaplan-Meier survival analysis. n = 8–9 mice per group. $^*P < 0.05$, Kruskal-Wallis test (**A** and **C**); log-rank test (**B** and **D**).

To address this question, we first treated human TLR9-expressing 293T cells with escalating doses of the TLR9 ligand, CpG ODN, in the presence or absence of PG545. Culture supernatants were then assayed for the induction of IL-8 production upon TLR9 activation. Increasing IL-8 levels were detected in TLR9-expressing 293T cells by CpG in a dose-dependent manner (Figure 6A). Interestingly, the presence of PG545 significantly enhanced TLR9 activation by low-dose CpG (0.1 and 1 μg/ml) (Figure 6A). In the absence of CpG, PG545 treatment did not increase IL-8 levels. No IL-8 was produced by control 293T cells stimulated with the highest dose (10 μg/ml) of CpG, confirming the specificity of TLR9 stimulation by CpG.

Since conventional $CD11c^+$ DCs have been shown to play a critical role in NK cell activation (30, 31), we next tested whether PG545 could enhance the activation of TLR9 on DCs. $CD11c^+$ bone marrow–derived DCs (BMDCs) of WT mice were treated with PG545 (5 μg/ml) alone or PG545 plus low-dose CpG (0.3 μg/ml) or high-dose CpG (3 μg/ml). Expression profiling of inflammatory cytokines was then performed by quantitative RT-PCR. PG545 did not activate DCs in the absence of CpG but significantly enhanced their response to CpG, especially at low-dose CpG concentrations (Figure 6B). At the protein level, we similarly observed that PG545 markedly enhanced the production of IL-12, IL-6, and TNF-α by WT but not *Tlr9*$^{-/-}$ DCs (Figure 6, C–E). In contrast, identical studies examining the production of type I IFNs (IFN-α and IFN-β) by DCs in response to CpG demonstrated that PG545 treatment actually decreased their production (Supplemental Figure 4). In all cases, no cytokine production was found in the absence of CpG, confirming that PG545 alone does not activate DCs directly. Taken together, these results indicate that PG545 enhances CpG-mediated TLR9 activation on DCs, leading to the enhanced production of proinflammatory cytokines.

To determine whether DCs were critical for the in vivo function of PG545 in activating NK cells and producing an inflammatory cytokine response, we treated CD11c–diphtheria toxin receptor (DTR) mice with diphtheria toxin to deplete $CD11c^+$ DCs prior to treatment with PG545 (Supplemental Figure 5). Following the in vivo depletion of $CD11c^+$ cells, PG545 was unable to upregulate NK expression of CD69, Ki-67, or IFN-γ. These data provide supporting evidence that $CD11c^+$ DCs are necessary for PG545-mediated NK cell activation in vivo.

PG545 promotes lysosomal accumulation of CpG in DCs. How does PG545 promote CpG-mediated activation of TLR9 on DCs? Studies have shown that CpG interacts with TLR9 in the endolysosomal compartment, in which it initiates downstream signal transduction (32, 33). Sensing of CpG in the endosome triggers the activation of IRF-7 and the production of type I IFNs, whereas lysosomal sensing of CpG is associated with NF-κB activation, leading to the expression of proinflammatory cytokines, such as IL-6,

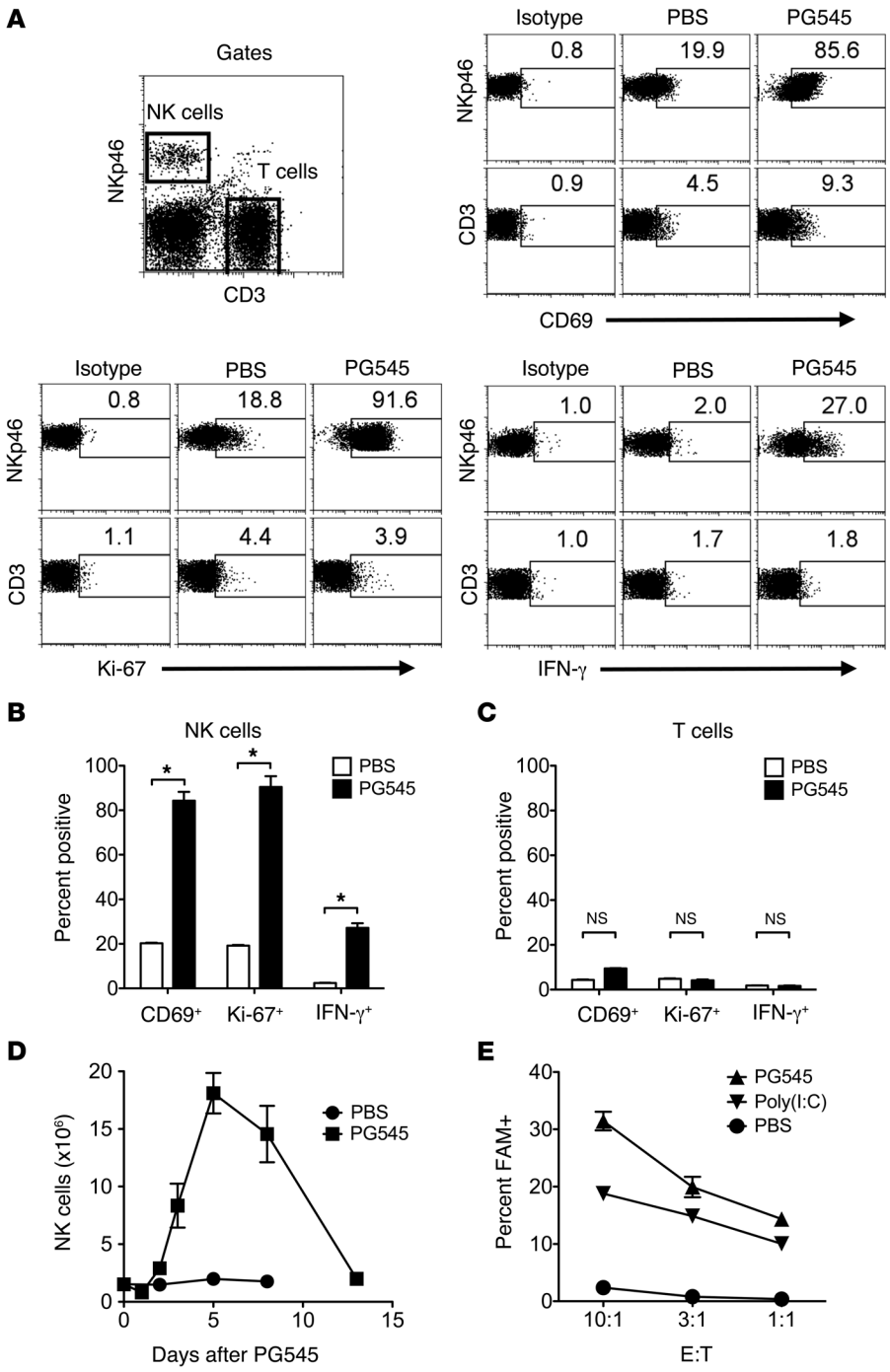

Figure 3. PG545 activates NK cells. (**A**–**C**) NK cells (NKp46$^+$CD3$^-$) and T cells (NKp46$^-$CD3$^+$) from BALB/c mice were FACS analyzed 2 days after injection of a single dose of PG545 (20 mg/kg, s.c.) for the expression of CD69, Ki-67, and IFN-γ. The percentage of CD69$^+$, Ki-67$^+$, or IFN-γ$^+$ cells among total NKp46$^+$ NK or CD3$^+$ T cells is indicated. (**D**) Total splenic NK cells were assessed over time following a single injection of PG545 and compared with PBS injection alone. (**E**) Ex vivo cytotoxicity assay. Purified NK cells from mice treated 2 days previously with PG545 (20 mg/kg, s.c.) or Poly(I:C) (200 μg, i.p.) were cocultured with NK-sensitive Yac-1 target cells at the indicated effector-to-target ratios (E/T) for 3 hours. Target cell cytotoxicity was assessed by FACS detection of the caspase-3 and -7 substrate, FAM. The percentage of apoptotic cells (FAM$^+$) is indicated. *$P < 0.05$, 2-tailed Student's *t* test.

IL-12, and TNF-α. The observed enhancement of CpG-dependent proinflammatory cytokine production by PG545, along with the suppression of type I IFN production, suggested that PG545 might promote the accumulation of CpG in the lysosomal compartment.

To address this question, BMDCs were cultured with FITC-labeled CpG in the presence or absence of PG545 (5 μg/ml) and analyzed by FACS. As shown in Figure 7A, PG545 increased the accumulation of CpG in DCs. Using confocal microscopy, we tested whether PG545 promoted the accumulation of CpG in the lysosomal compartment of DCs. DCs were cultured with Cy5-labeled CpG in the presence or absence of PG545. Intracellular localization of CpG was then compared with the localization of Alexa Fluor 488–labeled dextran as an endosomal marker and LysoTracker as a lysosomal marker. We found that the accumulation of CpG was colocalized to the lysosomal (Figure 7B), but not the endosomal (Figure 7C), compartment. To further confirm the colocalization of CpG with the lysosomal marker, we expressed GFP-labeled lysosomal-associated membrane protein 1 (LAMP-1) in the DC line, DC2.4, as a specific lysosomal marker. These cells were then treated with CpG-Cy5 with or without PG545 (Figure 7D). We found that PG545 stimulated the uptake and colocalization of CpG with LAMP-1, indicating that PG545 promotes lysosomal accumulation of CpG.

Next, we tested whether lysosomal function was necessary for the PG545-mediated DC activation in response to CpG. For this purpose, we tested a lysosomal inhibitor, chloroquine (CQ), in coculture with DCs with low-dose CpG (0.3 μg/ml) and with or without PG545. We found that the ability of PG545 to increase the response to CpG was completely inhibited by CQ (Supplemental Figure 6). As expected, LPS, a TLR4 agonist that does not signal through lysosomal pathways, was unaffected by CQ. Taken together, these data suggest that PG545 increased the accumulation of CpG ODNs in the lysosome and that lysosomal function is necessary for the immunostimulatory effect of PG545.

TLR9-dependent production of IL-12 is critical for PG545-mediated NK cell activation in vivo. Among proinflammatory cytokines produced by DCs, IL-12 has been shown to be a critical mediator of NK cell activation (34–37). We therefore examined whether PG545 caused DCs to produce IL-12 in vivo. WT, *Tlr9*$^{-/-}$, and

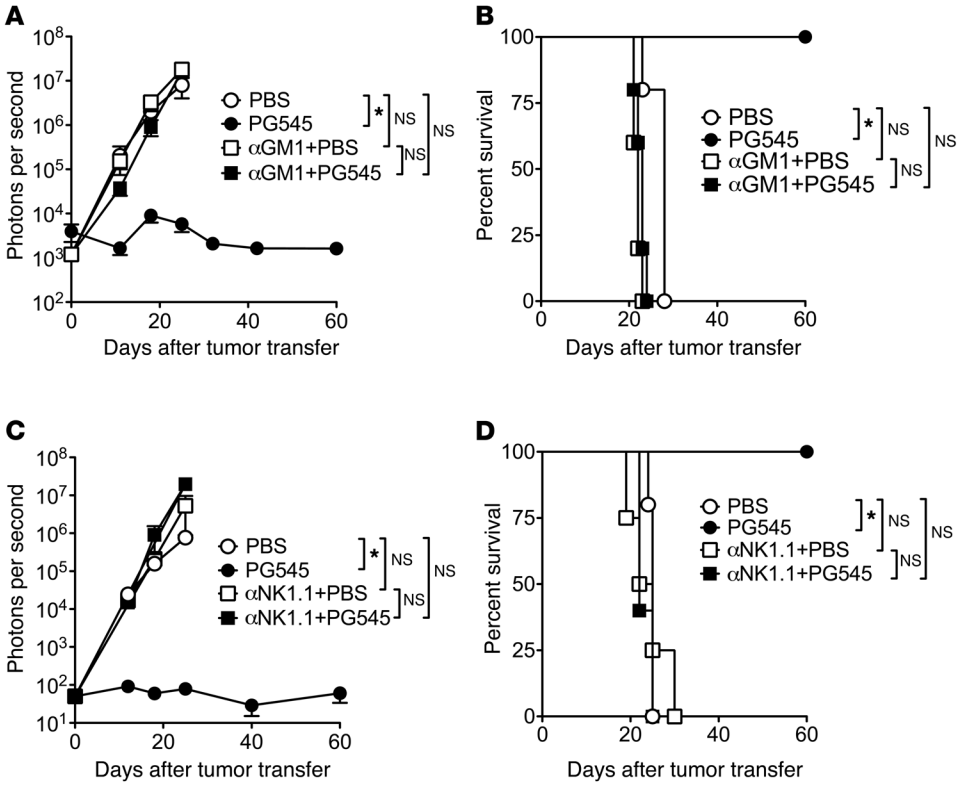

Figure 4. Antitumor activity of PG545 is dependent on NK cells. (**A** and **B**) BALB/c and (**C** and **D**) C57BL/6 mice were NK depleted by twice-weekly injections of anti-asialo GM1 (αGM1) and anti-NK1.1 (αNK1.1) antibody beginning 4 days prior to inoculation with 2×10^5 A20-luciferase and 1×10^5 EL-4-luciferase lymphoma cells, respectively. Mice were then treated with weekly injections of PG545 (20 mg/kg, s.c.) or PBS. NK depletion was determined at 2 weeks following tumor injection for BALB/c and C57BL/6 mice. (**A** and **C**) Tumor growth was assessed luminescence following D-luciferin injection. (**B** and **D**) Survival of tumor-bearing mice was compared by Kaplan-Meier survival analysis. n = 4–5 mice per group. $^*P < 0.05$, Kruskal-Wallis test (**A** and **C**); log-rank test (**B** and **D**).

Myd88$^{-/-}$ mice were treated with PG545, and CD11c$^+$ splenic DCs were analyzed for IL-12 production by intracellular staining and FACS analysis 2 days later. Consistent with in vitro results (Figure 6, B and C), PG545 also promoted DCs to produce IL-12 in vivo in a TLR9- and MyD88-dependent manner (Figure 8, A and B).

We next investigated whether IL-12 is critical for PG545-dependent NK cell activation in vivo. WT and *Il12*$^{-/-}$ mice were treated with PG545, and NK cell activation was examined 2 days later. We found that, compared with those in WT mice, the upregulation of CD69 and the production of IFN-γ were essentially abolished in *Il12*$^{-/-}$ mice (Figure 8, C and D), suggesting a critical role for IL-12 production in PG545-mediated NK cell activation in vivo.

DNA-binding polymers abrogate the in vivo effect of PG545 on NK cell activation. The observation that PG545 enhances CpG-mediated activation of TLR9 on DCs in vitro (Figure 6) suggested that the in vivo effect of PG545 could be mediated through endogenous TLR9 activating CpG DNA. To test this, we examined whether coadministration of hexadimethrine bromide (HDMBr), a nucleic acid–binding polymer (38), would eliminate the stimulatory effect of PG545 on splenic DCs and NK cells in vivo. Indeed, we found that HDMBr prevented PG545-induced IL-12 production by DCs (Figure 9, A and B) as well as the upregulation of CD69, Ki-67, and IFN-γ by NK cells (Figure 9, C and D). These results suggest that the immunostimulatory effect of PG545 on DCs and NK cells in vivo is mediated through an endogenous source of DNA.

Discussion

In this study, we showed that the in vivo antitumor effect of PG545, an antitumor therapy designed as an HS mimetic, is dependent on the activation of NK cells in murine models of B cell and T cell lymphomas and that NK cell activation by PG545 is mediated through the TLR9/MyD88 pathway. Mechanistically, we demonstrated that PG545 markedly enhances CpG-mediated activation of TLR9 on DCs by promoting the accumulation of CpG in the lysosomal compartment, leading to enhanced production of proinflammatory cytokines such as IL-12. We further demonstrated that TLR9-dependent production of IL-12 plays an essential role in PG545-mediated NK cell activation in vivo. Overall, these results uncover a function for PG545 in activating NK cells, which is critical for the antitumor effect of PG545 in these lymphoma models.

HS mimetics such as PG545 have been emerging as a promising class of antitumor agents (12, 17, 39). It has been previously demonstrated that the antitumor activity of HS mimetics is primarily mediated through the inhibition of growth factor binding and heparanase activity, which primarily effect tumor angiogenesis and metastasis (13, 14, 16, 22, 23, 40, 41). However, the potential effects of PG545 as an immunomodulatory agent have not been examined. Here, we provided the first evidence to our knowledge that the antitumor effect of PG545 in vivo is dependent on the activation of NK cells in murine models of B cell and T cell lymphomas. This mechanism of NK cell activation by PG545 and the previously identified mechanisms of antiangiogenic and antimetastatic activity are not mutually exclusive. Rather, our findings support a critical role for NK cell activation in the PG545-mediated antitumor effect. However, it remains to be determined whether PG545-mediated NK cell activation is also an important component of the antitumor effect of PG545 in solid tumors.

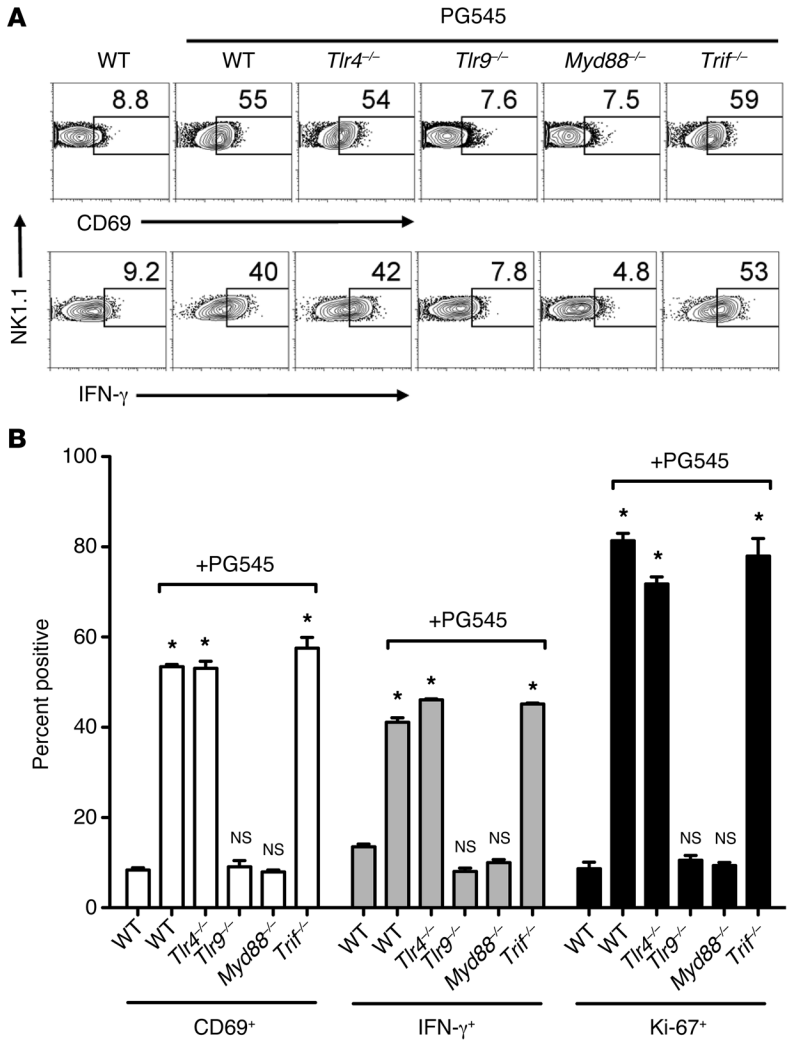

Figure 5. The TLR9/MyD88 pathway is required for in vivo PG545-dependent NK cell activation. WT, *Tlr4*$^{-/-}$, *Tlr9*$^{-/-}$, *Myd88*$^{-/-}$, and *Trif*$^{-/-}$ C57BL/6 mice were injected with PG545 (20 mg/kg, s.c.). Two days later, splenic NK cells (NK1.1$^+$CD3$^-$) were FACS analyzed for markers of activation and proliferation. (**A**) Representative FACS plots for CD69 expression and IFN-γ production by NK cells, with percentage of CD69$^+$ and IFN-γ$^+$ NK cells among total splenic NK cells indicated. (**B**) The mean percentage ± SEM of CD69$^+$, IFN-γ$^+$, or Ki-67$^+$ NK cells among total splenic NK cells is shown (n = 3 mice per group). *P < 0.05, 2-tailed Student's t test.

The observation that the activation of NK cells by PG545 is dependent on the TLR9/MyD88 pathway in vivo is consistent with the important role of the TLR9/MyD88 pathway in NK cell activation and function in various models of viral infection (26, 42–44). However, in contrast to these models of viral infection in which TLR9-dependent production of type I IFNs by DCs is critical to the mediation of NK cell activation, we showed that TLR9-dependent production of IL-12 by DCs is necessary for PG545-mediated NK cell activation. What contributes to the discrepancy? Studies have shown that, after binding to CpG, TLR9 undergoes a conformational change that leads to recruitment of MyD88. Interactions of TLR9 with MyD88 in the endosome lead to the activation of IRF-7 and the production of type I IFNs (33), whereas interactions of TLR9 with MyD88 in the lysosomal compartment lead to activation of the MAPK pathway, NF-κB nuclear translocation, and the production of inflammatory cytokines, such as IL-12, IL-6, and TNF-α. Indeed, our in vitro studies demonstrated that PG545 did not directly activate TLR9 on DCs, but instead enhanced the accumulation of CpG in the lysosomal compartment of DCs, leading to increased IL-12 production, which is critical for PG545-mediated NK cell activation in vivo. The mechanism by which PG545 promotes the accumulation of CpG DNA in lysosomes requires further investigation. Considering the polyanionic nature of the highly sulfated PG545 and the phosphate backbone of DNA, it is unlikely that these molecules directly interact.

How PG545 promotes NK cell action in vivo remains unknown. Our finding that coadministration of HDMBr, a nucleic acid–binding polymer (38), abolishes PG545-induced IL-12 production by DCs as well as NK cell activation in vivo suggested that the in vivo effect of PG545 might be mediated by an endogenous source of CpG DNA. The origin of the endogenous TLR9 ligand that PG545 enhances remains to be determined. Endogenous CpG DNA could be derived from cell necrosis or apoptosis. However, NK cells have been shown to be activated by DNA from bacteria or viruses, not from vertebrates (45). This is due to the presence of unmethylated CpG motifs (46, 47). Theoretically, endogenous CpG could originate from bacterial genomic DNA from intestinal or pulmonary flora that enter the circulation or from chronic viral infections. Another source of endogenous CpG could be mitochondrial DNA released into the extracellular milieu as the result of cell injury (48) or through a dysregulation of autophagy (49, 50). Mitochondria evolved from a symbiotic relationship between aerobic bacteria and primordial eukaryotic cells (51) and, consequently, retained unmethylated CpG sequences that can cause inflammation (48, 52). Thus, further studies are needed to identify the source of endogenous CpG DNA in the future.

NK cells play an important role in the host's immunological defense against malignancies, and adjuvant therapies designed to enhance NK activation and cytotoxicity are promising antitumor strategies. We believe our results reveal PG545 as a novel and effective NK activating agent for the treatment of lymphomas. This is achieved by enhancing TLR9 activation and IL-12 production. It is reasonable to predict that PG545 can be developed as an antilymphoma agent used with cytoreduction therapy and/or used in combination with synthetic CpG ODN to achieve maximal NK cell activation and antitumor effect. Indeed, CpG ODNs have been investigated as potential antitumor therapeutic reagents. These reagents, typically modified with phosphorothioate bonds to protect against nucleases and improve in vivo half-life, are currently

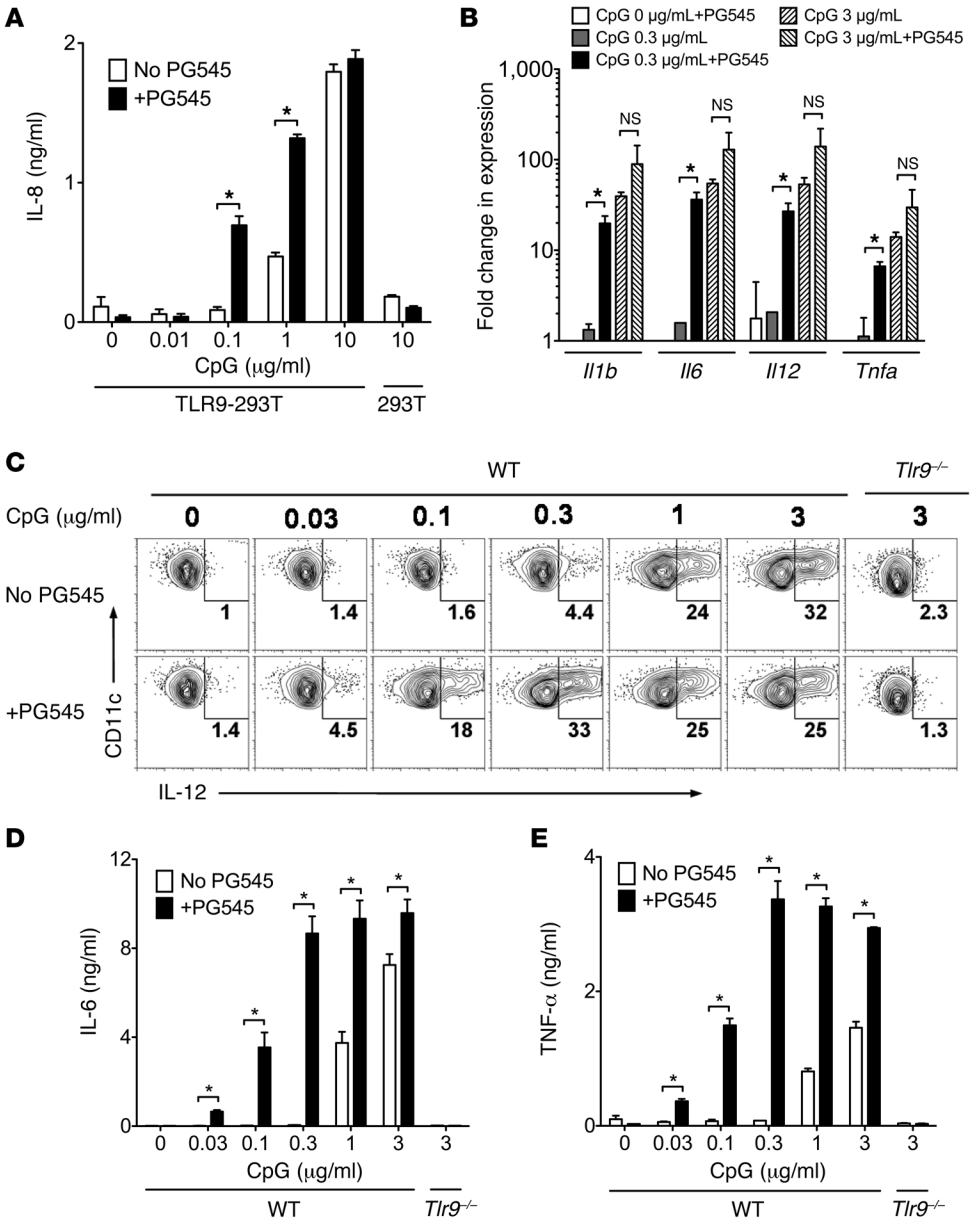

Figure 6. PG545 enhances CpG-mediated activation of TLR9. (**A**) HEK 293T cells stably expressing human TLR9 were treated with increasing concentrations of CpG (ODN 2395) in the presence (+PG545) or absence (No PG545) of PG545 (5 μg/ml). As a control, 293T cells not expressing human TLR9 were assayed at the highest CpG concentration (10 μg/ml). 18 hours later, culture supernatants were assayed for IL-8 production by ELISA. (**B**) Quantitative RT-PCR was performed on cDNA obtained from BMDCs incubated for 18 hours with low-dose (0.3 μg/ml) or high-dose (3 μg/ml) CpG in the presence of absence of PG545 (5 μg/ml). Fold change in expression over the no-treatment reference sample, normalized to reference genes *Gapdh* and β-actin, is shown for triplicate samples. (**C**–**E**) WT and *Tlr9*$^{-/-}$ BMDCs were treated with increasing concentrations of CpG in the presence or absence of PG545 (5 μg/ml). 18 hours later, DCs were analyzed for IL-12 production by intracellular staining. (**C**) The percentage of IL-12–producing DCs among CD11c^{+} DCs is shown. Culture supernatants were assayed for the secretion of (**D**) IL-6 and (**E**) TNF-α by ELISA. Data are representative of 3 independent experiments. *$P < 0.05$, 2-tailed Student's *t* test.

being tested in multiple phase II and phase III human clinical trials as adjuvants to cancer vaccines and in combination with conventional chemotherapy against many tumor types, including trials against human lymphoma and leukemia (53, 54). The activation of NK cells by PG545 via enhancement of TLR9 pathways should further enhance the potency of CpG for the treatment of malignancies (55).

In conclusion, we have revealed a function for PG545 in NK cell activation and function, which is critical for the antitumor effect of PG545 in vivo. We have demonstrated that PG545-dependent NK cell activation in vivo is mediated by the TLR9/MyD88 pathway and that PG545 enhances TLR9 activation on DCs by promoting the accumulation of CpG in the lysosomal compartment, leading to enhanced production of IL-12, which is critical for PG545-mediated NK cell activation in vivo. Overall, these findings may have important implications in improving NK cell–based antitumor therapies.

Methods

Mice. BALB/c and C57BL/6 mice were purchased from the National Cancer Institute. *Myd88*$^{-/-}$, *Trif*$^{-/-}$, *Tlr9*$^{-/-}$, *Tlr4*$^{-/-}$, *Il12*$^{-/-}$, and CD11c-DTR C57BL/6 mice were purchased from The Jackson Laboratory.

Cell lines and reagents. Unless otherwise stated, all cell culture media were obtained from Life Technologies. HEK 293 (CRL-1573), 293T (CRL-11268), A20 (TIB-208), EL-4 (TIB-39), and Yac-1 (TIB-160) cells were obtained from the ATCC. The DC line, DC2.4, was a gift from Kenneth Rock at the University of Massachusetts Medical School, Worcester, Massachusetts, USA. HEK 293 cell lines coexpressing human TLR9 were purchased from InvivoGen. Cell lines were cultured in DMEM media supplemented with 10% FCS and penicillin and streptomycin. BMDCs were cultured from bone marrow collected from the tibia and femur in the presence of mouse GM-CSF (1,000 U/ml, R&D Systems Inc.) in complete RPMI 1640 medium (10% heat-inactivated FCS, 25 mM HEPES, 50 μM 2-ME, 2 mM L-glutamine, 100 IU/ml penicillin, and 100 IU/ml streptomycin)

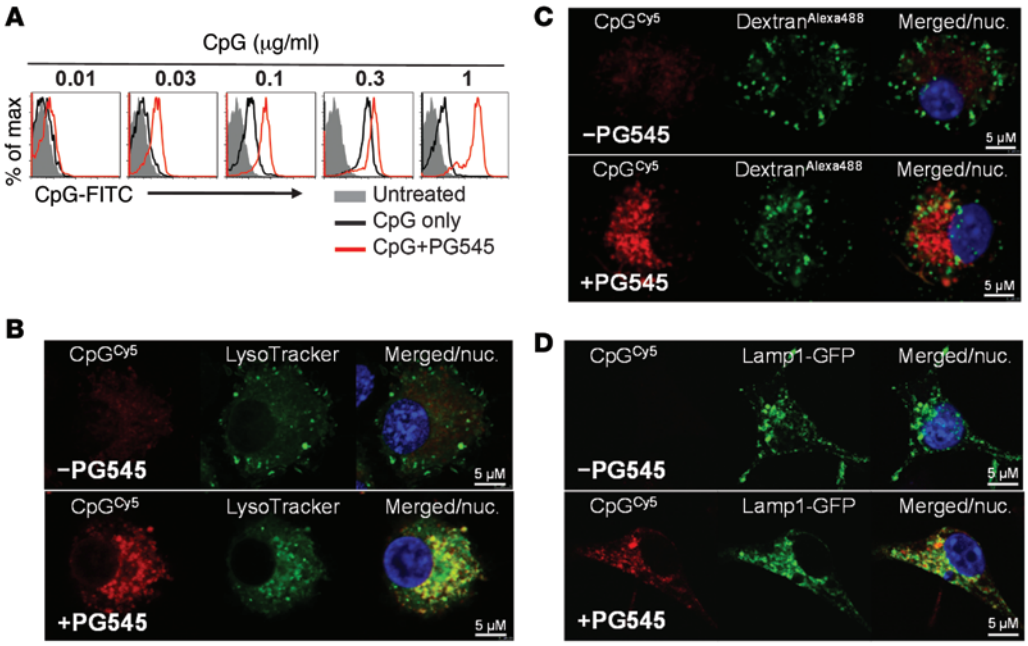

Figure 7. PG545 promotes the accumulation of CpG in the lysosomal compartment of DCs. (**A**) BMDCs were incubated with various concentrations of FITC-labeled CpG in the presence (CpG+PG545) or absence (CpG only) of PG545 (5 μg/ml), and the uptake of FITC-labeled CpG was analyzed by FACS 6 hours later. Cells without CpG treatment (Untreated) were used as a control. Representative plots from 3 independent experiments are shown. (**B** and **C**) DCs were treated with Cy5-labeled (red) CpG (0.3 μg/ml) for 90 minutes in the presence or absence of PG545 (5 μg/ml). Cells were then stained with (**B**) LysoTracker (green), a lysosome marker, or (**C**) Alexa Fluor 488–labeled dextran (green), an endosome marker (**C**), as well as nuclear staining with Hoechst 33342 (blue) and imaged by confocal microscopy. Representative images of DCs with CpG, dextran, or LysoTracker as well as merged images of CpG with dextran or LysoTracker are shown. (**D**) DC2.4 cells were transfected with LAMP-1-GFP and treated with CpG-Cy5 (0.3 μg/ml) for 90 minutes in the presence or absence of PG545 (5 μg/ml). Representative images of LAMP-1-GFP–transfected (green) DCs with CpG (red) as well as merged images with nuclear staining are shown. Scale bar: 5 μm.

for 5 days as described previously (56), and $CD11c^+$ DCs were purified using a FACS Diva cell sorter (BD Biosciences).

Unlabeled and Cy5-labeled ODN 2395 was synthesized by Integrated DNA Technologies. The sequence of ODN 2395 is 5′-TCGTCGTTTTCGGCGCGCGCCG-3′, with a fully phosphorothioate-modified backbone. FITC-labeled ODN 2395 was purchased from InvivoGen. Poly(I:C), LPS, CQ, and HDMBr were from Sigma-Aldrich. CP was purchased from Bristol-Myers Squibb.

Generation of luciferase-expressing lymphoma cell lines. A bicistronic lentiviral-based vector encoding for firefly luciferase (Luc2) and GFP linked by an internal ribosomal entry site (IRES) was made by subcloning Luc2.IRES.GFP from the retroviral vector rKat.Luc2.IRES.GFP (57) in front of the ubiquitin promoter of a previously described lentiviral vector (58). Lentiviral particles were packaged in 293T cells using Δ8.9 and pCMV-VSVg and concentrated by centrifugation as described previously (58, 59). Murine B cell (A20) and T cell (EL-4) lymphoma cell lines were transduced with lentivirus in the presence of 6 μg/ml Polybrene (Sigma-Aldrich) for 90 minutes during centrifugation at 1,200 at 23°C. Transduced cells underwent single-cell sorting for GFP, and A20-Luc2/GFP and EL-4-Luc2/GFP clones were tested for luciferase expression using the Bright-Glo Luciferase Assay system, as per the manufacturer's instructions (Promega).

In vivo lymphoma models. BALB/c and C57BL/6 mice were inoculated with A20-Luc2/GFP lymphoma cells intravenously or with EL-4-Luc2/GFP lymphoma cells subcutaneously. BALB/c mice were preconditioned with 4 Gy of total body irradiation 2 to 4 hours prior to tumor administration as previously described (57). Mice were then treated with once weekly subcutaneous dosing of PG545 (20 mg/kg; Progen Pharmaceuticals Limited). Tumor burden was quantified by measuring luciferase activity after i.p. injection of D-Luciferin (150 μg per gram body weight, Gold BioTechnology Inc.) using an in vivo imaging system (IVIS) (IVIS 100, PerkinElmer). End points for survival were death, moribund status, hind-limb paralysis, palpable tumor >2 cm in diameter, or weight loss ≥30%. In the established tumor model, A20-luciferase tumor growth in vivo was monitored by IVIS until the tumor was visualized (photons per second flux of ~10^5), at which point mice were treated with 50 mg/kg CP i.p., with or without weekly s.c. injections of PG545 (20 mg/kg). To deplete NK cells in BALB/c mice, 50 μl rabbit anti-asialo GM1 (Wako Pure Chemical Industries Ltd.) was injected i.p. 2 and 4 days prior to tumor inoculation and then twice weekly for 2 weeks. To deplete NK cells in C57BL/6 mice, 200 μg anti-NK1.1 (PK136) was injected i.p. 2 and 4 days prior to tumor inoculation and then twice weekly for 2 weeks. Depletion of NK cells was determined by FACS analysis for $NKp46^+CD3^-$ cells.

Flow cytometry. Anti-CD40 (HM40-3), CD86 (GL1), CD3ε (145-2C11), NK1.1 (PK136), DX5 (DX5), CD11c (HL3), B220 (RA3-682), CD69 (H1.2F3), Sca-1 (E13-161.7), CD107a (1D4B), IL-12 (C15.6), Ly5.1 (A20), IFN-γ (XMG1.2), hamster IgM isotype (G235-1), hamster IgG1 isotype (G235-2356), rat IgG2a isotype (R35-95), and rat IgG1 isotype (R3-34) were from BD Biosciences. Anti–Ki-67 (SolA15) was from eBioscience Inc. Flow cytometric data were acquired using a FACSCanto flow cytometer (BD Biosciences), and events were analyzed using FlowJo Version 9.3 software (TreeStar).

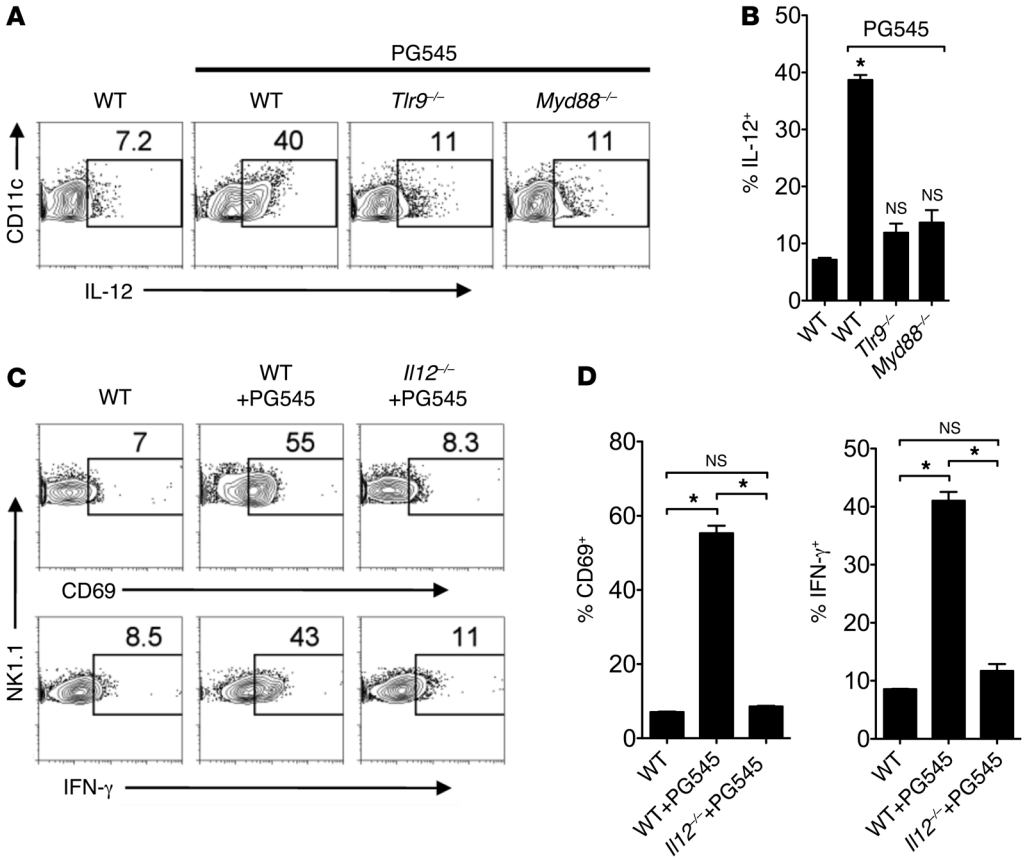

Figure 8. IL-12 is necessary for NK cell activation by PG545 in vivo. WT, *Tlr9*$^{-/-}$, and *Myd88*$^{-/-}$ C57BL/6 mice were injected with PG545 (20 mg/kg, s.c.), and splenic CD11c$^+$ DCs were analyzed by FACS for IL-12 production 2 days later. Untreated WT mice were used as a control. (**A**) Representative FACS plots with the percentage of IL-12–producing cells indicated. (**B**) The mean percentage ± SEM of IL-12–producing cells among CD11c$^+$ DCs is shown (n = 3 per group). (**C**) WT and *Il12*$^{-/-}$ C57BL/6 mice were injected with PG545 (20 mg/kg, s.c.), and splenic NK cells (NK1.1$^+$CD3$^-$) were analyzed for CD69 expression and IFN-γ production 2 days later. Representative FACS plots with the percentage of CD69$^+$ or IFN-γ$^+$ cells indicated. (**D**) The mean percentage ± SEM of CD69$^+$ or IFN-γ$^+$ cells among NK cells is shown (n = 3 per group). *$P < 0.05$, 2-tailed Student's t test.

Measurement of inflammatory cytokines. DC culture supernatants were assayed for the secretion of IL-6 and TNF-α by ELISA (BD Biosciences). Intracellular staining for IFN-γ was performed following ex vivo stimulation of splenocytes for 6 hours with 20 ng/ml PMA and 50 ng/ml ionomycin in the presence of 5 μg/ml brefeldin A. Intracellular staining for IL-12 was performed as previously described (60). Intracellular staining for IFN-γ and IL-12 was performed following treatment with Cytofix/Cytoperm (BD Biosciences) solution. Supernatants from 293T cultures were tested for human IL-8 by ELISA (BD Biosciences). ELISA kits from BD Biosciences were used to quantify IL-6, TNF-α, and IL-8 in cell culture supernatant. ELISA kits from PBL Assay Science were used to quantify IFN-α and IFN-β in cell culture supernatant. An Inflammatory Cytometric Bead Array Kit from BD Biosciences was used to quantify serum levels of IFN-γ, MCP-1, and TNF-α.

RT-PCR. Total RNA was isolated from mouse BMDCs using the Absolutely RNA Miniprep Kit (Agilent Technologies) according to the manufacturer's recommendations. Genomic DNA contamination was eliminated by treatment with DNAse I (Life Technologies). cDNA was reverse transcribed using SuperScript II and Oligo(dT) 12-18 primers (Life Technologies). Quantitative RT-PCR was then performed using Mouse Toll-Like Receptor Signaling Pathway RT^2 Profiler PCR Arrays and RT^2 Real-Time SyBR Green/ROX PCR Mix according to the manufacturer's protocol (Qiagen). PCR was performed with the MyiQ Real-Time PCR Detection System (Bio-Rad) according to the manufacturer's instructions. For data analysis, the ΔΔCt method was used with the aid of a Microsoft Excel spreadsheet containing algorithms provided by the manufacturer. Fold changes were then calculated and expressed as log-normalized ratios of values from PG545- and CpG-treated DCs compared with untreated DCs.

Cytotoxicity assays. An in vitro cytotoxicity assay was performed using a 3-hour coculture of Yac-1 cells (1×10^4) labeled with 0.6 μM 7-hydroxy-9*H*-(1,3-dichloro-9,9-dimethylacridin-2-one) (Life Technologies), with varying ratios of NK cells purified from the spleens of mice injected with PG545 (20 mg/kg, s.c.) or Poly(I:C) (200 μg, i.p.) 2 days prior. NK cells were purified with anti-PE beads (Miltenyi) following DX5-PE staining of splenocytes. Cytotoxic activity was determined using the Vybrant FAM Caspase-3 and -7 Assay Kit (Life Technologies) according to the manufacturer's protocol.

Immunohistology. Cryostat sections (10 μM) were dried, fixed in methanol, and incubated for 1 hour in blocking buffer (0.1 M Tris, 0.05 M NaPhos, 0.3% Tween 20, 3% goat serum). Intrinsic peroxidase activity was blocked by incubation in 0.3% H_2O_2 in PBS for 5 minutes at room temperature. Slides were coincubated with purified rat IgM anti-CD49b

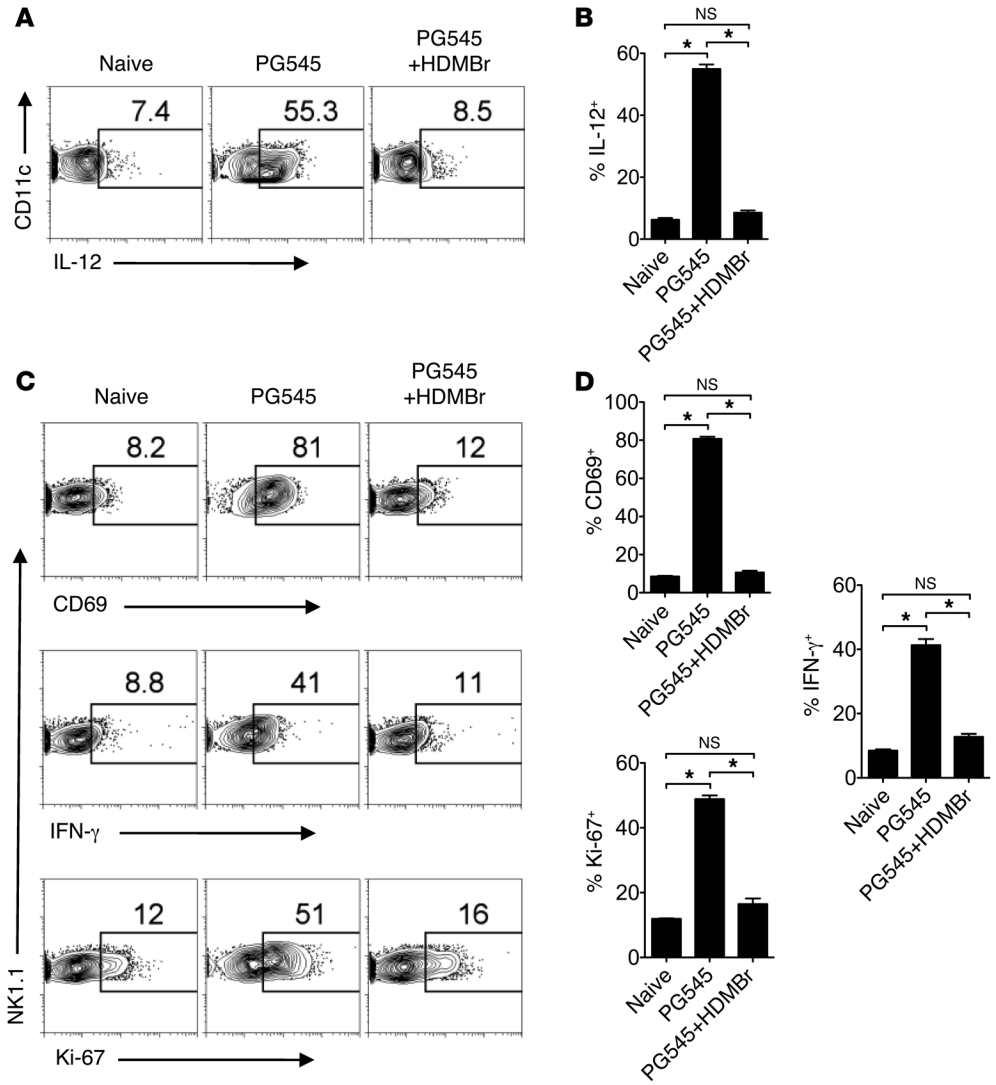

Figure 9. Nucleic acid–binding polymer abrogates activation of NK cells by PG545 in vivo. Mice were treated with PG545 (20 mg/kg, i.p.) or PG545 along with HDMBr (200 μg, i.p.) (PG545+HDMBr). Some mice were left untreated as a control (naive). Splenic CD11c$^+$ DCs were analyzed by FACS for IL-12 production 2 days later. (**A**) Representative FACS plots with the percentage of IL-12–producing cells indicated. (**B**) The mean percentage ± SEM of IL-12–producing cells among CD11c$^+$ DCs is shown (n = 3 mice per group). Splenic NK cells (NK1.1$^+$CD3$^-$) were analyzed for CD69, IFN-γ, and Ki-67 expression 2 days following injection of PG545 or injection of PG545 and HDMBr. (**C**) Representative FACS plots of CD69, IFN-γ, and Ki-67 staining are shown. (**D**) The mean percentage ± SEM of CD69$^+$, IFN-γ$^+$, or Ki-67$^+$ cells among NK cells is shown (n = 3 mice per group). *P < 0.05, 2-tailed Student's t test.

(DX5, BD Pharmingen, 1:30) and rat IgG anti-CD45R (RA3-6B2, BD Pharmingen, 1:100) overnight at 4°C in blocking buffer and subsequently with alkaline phosphatase–conjugated anti-rat IgM (Jackson ImmunoResearch, 112-055-075, 1:200) and peroxidase-conjugated anti-rat IgG (Jackson ImmunoResearch, 712-035-153, 1:200) for 30 minutes at room temperature. Slides were then developed with alkaline phosphatase substrate (SK-5100, Vector Labs) and diaminobenzidine substrate (SK-4105, Vector Labs) and counterstained with methyl green nuclear counterstain (H-3402, Vector Labs).

BMDCs were cultured at 37°C on poly-D-lysine–coated coverslips (BD Biosciences) in 24-well plates with 0.3 μg/ml Cy5-labeled CpG for 90 minutes. Cells were stained with 1 μg/ml Hoechst 33342 for 30 minutes and either Alexa Fluor 488–labeled 10,000-MW dextran or LysoTracker Red (Life Technologies) at final concentrations of 250 μg/ml and 100 nM, respectively, for 10 minutes. DC2.4 cells were transfected with LAMP1-mGFP reporter plasmid (a gift from Esteban Dell'Angelica; Addgene plasmid 34831) using Lipofectamine (Life Technologies) and imaged 2 days after transfection.

Imaging. Images were acquired using a Leica SP5 AOBS confocal microscope (Leica Microsystems) equipped with an ×40 (1.25 NA) oil immersion objective. 405-nm, 488-nm, 561-nm, and 633-nm lasers were used to excite Hoechst, Alexa Fluor 488–labeled dextran, LysoTracker Red, and Cy5-labeled CpG, respectively. Sequential acquisition of the multicolor images was used to avoid cross-excitation, and images were overlaid with the Leica LAS AF 2.6 software.

Statistics. Results are expressed as mean ± SEM. Comparison between groups was performed by Kruskal-Wallis and 2-tailed Student's t test for continuous variables and log-rank test for survival data. All statistical analyses were performed using Prism Version 5.0 software (GraphPad Software). P values of less than 0.05 are considered to be significant.

Study approval. All experimental procedures involving the use of mice were done in accordance with protocols approved by the Animal Care and Use Committee of Duke University.

Author contributions

TVB designed and performed research, collected and analyzed data, and wrote the paper; LL, JDB, and VRR performed research and collected and analyzed data; KD analyzed data and wrote the paper; and XH and YY designed research, analyzed data, and wrote the paper.

Acknowledgments

This work was supported by NIH grants CA136934 (to Y. Yang), CA047741 (to Y. Yang), AI083000 (to Y. Yang), and AI101263 (to T.V. Brennan).

Address correspondence to: Yiping Yang, Department of Medicine, Duke University Medical Center, Box 103005, Durham, North Carolina 27710, USA. Phone: 919.668.0932; E-mail: yang0029@mc.duke.edu.

1. Wegrowski Y, Maquart FX. Involvement of stromal proteoglycans in tumour progression. *Crit Rev Oncol Hematol*. 2004;49(3):259–268.
2. Sasisekharan R, Shriver Z, Venkataraman G, Narayanasami U. Roles of heparan-sulphate glycosaminoglycans in cancer. *Nat Rev Cancer*. 2002;2(7):521–528.
3. Bernfield M, et al. Functions of cell surface heparan sulfate proteoglycans. *Annu Rev Biochem*. 1999;68:729–777.
4. Dempsey LA, Brunn GJ, Platt JL. Heparanase, a potential regulator of cell-matrix interactions. *Trends Biochem Sci*. 2000;25(8):349–351.
5. Cohen I, et al. Heparanase promotes growth, angiogenesis and survival of primary breast tumors. *Int J Cancer*. 2006;118(7):1609–1617.
6. Maxhimer JB, et al. Heparanase-1 expression is associated with the metastatic potential of breast cancer. *Surgery*. 2002;132(2):326–333.
7. Mikami S, et al. Expression of heparanase in renal cell carcinomas: implications for tumor invasion and prognosis. *Clin Cancer Res*. 2008;14(19):6055–6061.
8. Lerner I, et al. Function of heparanase in prostate tumorigenesis: potential for therapy. *Clin Cancer Res*. 2008;14(3):668–676.
9. Koliopanos A, et al. Heparanase expression in primary and metastatic pancreatic cancer. *Cancer Res*. 2001;61(12):4655–4659.
10. Johnson GB, Brunn GJ, Kodaira Y, Platt JL. Receptor-mediated monitoring of tissue well-being via detection of soluble heparan sulfate by Toll-like receptor 4. *J Immunol*. 2002;168(10):5233–5239.
11. Brennan TV, et al. Heparan sulfate, an endogenous TLR4 agonist, promotes acute GVHD following allogeneic stem cell transplantation. *Blood*. 2012;120(14):2899–2908.
12. McKenzie EA. Heparanase: a target for drug discovery in cancer and inflammation. *Br J Pharmacol*. 2007;151(1):1–14.
13. Ferro V, et al. Discovery of PG545: a highly potent and simultaneous inhibitor of angiogenesis, tumor growth, and metastasis. *J Med Chem*. 2012;55(8):3804–3813.
14. Dredge K, et al. PG545, a dual heparanase and angiogenesis inhibitor, induces potent anti-tumour and anti-metastatic efficacy in preclinical models. *Br J Cancer*. 2011;104(4):635–642.
15. Hammond E, Li CP, Ferro V. Development of a colorimetric assay for heparanase activity suitable for kinetic analysis and inhibitor screening. *Anal Biochem*. 2010;396(1):112–116.
16. Ostapoff KT, et al. PG545, an angiogenesis and heparanase inhibitor, reduces primary tumor growth and metastasis in experimental pancreatic cancer. *Mol Cancer Ther*. 2013;12(7):1190–1201.
17. Zhou H, et al. M402, a novel heparan sulfate mimetic, targets multiple pathways implicated in tumor progression and metastasis. *PLoS One*. 2011;6(6):e21106.
18. Hammond E, Brandt R, Dredge K. PG545, a heparan sulfate mimetic, reduces heparanase expression in vivo, blocks spontaneous metastases and enhances overall survival in the 4T1 breast carcinoma model. *PLoS One*. 2012;7(12):e52175.
19. Basche M, et al. A phase I biological and pharmacologic study of the heparanase inhibitor PI-88 in patients with advanced solid tumors. *Clin Cancer Res*. 2006;12(18):5471–5480.
20. Johnstone KD, et al. Synthesis and biological evaluation of polysulfated oligosaccharide glycosides as inhibitors of angiogenesis and tumor growth. *J Med Chem*. 2010;53(4):1686–1699.
21. Liu CJ, et al. Heparanase inhibitor PI-88 as adjuvant therapy for hepatocellular carcinoma after curative resection: a randomized phase II trial for safety and optimal dosage. *J Hepatol*. 2009;50(5):958–968.
22. Joyce JA, Freeman C, Meyer-Morse N, Parish CR, Hanahan D. A functional heparan sulfate mimetic implicates both heparanase and heparan sulfate in tumor angiogenesis and invasion in a mouse model of multistage cancer. *Oncogene*. 2005;24(25):4037–4051.
23. Ferro V, et al. PI-88 and novel heparan sulfate mimetics inhibit angiogenesis. *Semin Thromb Hemost*. 2007;33(5):557–568.
24. Bitan M, et al. Heparanase upregulates Th2 cytokines, ameliorating experimental autoimmune encephalitis. *Mol Immunol*. 2010;47(10):1890–1898.
25. Barash U, et al. Proteoglycans in health and disease: new concepts for heparanase function in tumor progression and metastasis. *FEBS J*. 2010;277(19):3890–3903.
26. Krug A, et al. TLR9-dependent recognition of MCMV by IPC and DC generates coordinated cytokine responses that activate antiviral NK cell function. *Immunity*. 2004;21(1):107–119.
27. Johnson GB, Brunn GJ, Platt JL. Cutting edge: an endogenous pathway to systemic inflammatory response syndrome (SIRS)-like reactions through Toll-like receptor 4. *J Immunol*. 2004;172(1):20–24.
28. Kawai T, Akira S. The role of pattern-recognition receptors in innate immunity: update on Toll-like receptors. *Nat Immunol*. 2010;11(5):373–384.
29. Akira S, Takeda K. Toll-like receptor signalling. *Nat Rev Immunol*. 2004;4(7):499–511.
30. Andoniou CE, et al. Interaction between conventional dendritic cells and natural killer cells is integral to the activation of effective antiviral immunity. *Nat Immunol*. 2005;6(10):1011–1019.
31. Lucas M, Schachterle W, Oberle K, Aichele P, Diefenbach A. Dendritic cells prime natural killer cells by trans-presenting interleukin 15. *Immunity*. 2007;26(4):503–517.
32. Latz E, et al. TLR9 signals after translocating from the ER to CpG DNA in the lysosome. *Nat Immunol*. 2004;5(2):190–198.
33. Honda K, et al. Spatiotemporal regulation of MyD88-IRF-7 signalling for robust type-I interferon induction. *Nature*. 2005;434(7036):1035–1040.
34. Amakata Y, Fujiyama Y, Andoh A, Hodohara K, Bamba T. Mechanism of NK cell activation induced by coculture with dendritic cells derived from peripheral blood monocytes. *Clin Exp Immunol*. 2001;124(2):214–222.
35. Colonna M, Jonjic S, Watzl C. Natural killer cells: fighting viruses and much more. *Nat Immunol*. 2011;12(2):107–110.
36. Trinchieri G, Gerosa F. Immunoregulation by interleukin-12. *J Leukoc Biol*. 1996;59(4):505–511.
37. Colombo MP, Trinchieri G. Interleukin-12 in anti-tumor immunity and immunotherapy. *Cytokine Growth Factor Rev*. 2002;13(2):155–168.
38. Lee J, et al. Nucleic acid-binding polymers as anti-inflammatory agents. *Proc Natl Acad Sci USA*. 2011;108(34):14055–14060.
39. Ishida K, Wierzba MK, Teruya T, Simizu S, Osada H. Novel heparan sulfate mimetic compounds as antitumor agents. *Chem Biol*. 2004;11(3):367–377.
40. Dredge K, et al. The PG500 series: novel heparan sulfate mimetics as potent angiogenesis and heparanase inhibitors for cancer therapy. *Invest New Drugs*. 2010;28(3):276–283.
41. Hammond E, Handley P, Dredge K, Bytheway I. Mechanisms of heparanase inhibition by the heparan sulfate mimetic PG545 and three structural analogues. *FEBS Open Bio*. 2013;3:346–351.
42. Hochrein H, et al. Herpes simplex virus type-1 induces IFN-alpha production via Toll-like receptor 9-dependent and -independent pathways. *Proc Natl Acad Sci USA*. 2004;101(31):11416–11421.
43. Zhu J, Huang X, Yang Y. Innate immune response to adenoviral vectors is mediated by both Toll-like receptor-dependent and -independent pathways. *J Virol*. 2007;81(7):3170–3180.
44. Zhu J, Huang X, Yang Y. The TLR9-MyD88 pathway is critical for adaptive immune responses to adeno-associated virus gene therapy vectors in mice. *J Clin Invest*. 2009;119(8):2388–2398.

45. Yamamoto S, et al. DNA from bacteria, but not from vertebrates, induces interferons, activates natural killer cells and inhibits tumor growth. *Microbiol Immunol*. 1992;36(9):983–997.
46. Hemmi H, et al. A Toll-like receptor recognizes bacterial DNA. *Nature*. 2000;408(6813):740–745.
47. Krieg AM, et al. CpG motifs in bacterial DNA trigger direct B-cell activation. *Nature*. 1995;374(6522):546–549.
48. Zhang Q, et al. Circulating mitochondrial DAMPs cause inflammatory responses to injury. *Nature*. 2010;464(7285):104–107.
49. Deretic V. Autophagy in innate and adaptive immunity. *Trends Immunol*. 2005;26(10):523–528.
50. Oka T, et al. Mitochondrial DNA that escapes from autophagy causes inflammation and heart failure. *Nature*. 2012;485(7397):251–255.
51. Wallace DC. A mitochondrial paradigm of metabolic and degenerative diseases, aging, and cancer: a dawn for evolutionary medicine. *Annu Rev Genet*. 2005;39:359–407.
52. Escames G, et al. Mitochondrial DNA and inflammatory diseases. *Hum Genet*. 2012;131(2):161–173.
53. Krieg AM. Development of TLR9 agonists for cancer therapy. *J Clin Invest*. 2007;117(5):1184–1194.
54. Krieg AM. CpG still rocks! Update on an accidental drug. *Nucleic Acid Ther*. 2012;22(2):77–89.
55. Chinnathambi S, Chen S, Ganesan S, Hanagata N. Binding mode of CpG oligodeoxynucleotides to nanoparticles regulates bifurcated cytokine induction via Toll-like receptor 9. *Sci Rep*. 2012;2:534.
56. Yang Y, Huang C-T, Huang X, Pardoll DM. Persistent Toll-like receptor signals are required for reversal of regulatory T cell-mediated CD8 tolerance. *Nat Immunol*. 2004;5(5):508–515.
57. Cheadle EJ, et al. Natural expression of the CD19 antigen impacts the long-term engraftment but not antitumor activity of CD19-specific engineered T cells. *J Immunol*. 2010;184(4):1885–1896.
58. Lois C, Hong EJ, Pease S, Brown EJ, Baltimore D. Germline transmission and tissue-specific expression of transgenes delivered by lentiviral vectors. *Science*. 2002;295(5556):868–872.
59. Brennan TV, et al. A new T-cell receptor transgenic model of the CD4+ direct pathway: level of priming determines acute versus chronic rejection. *Transplantation*. 2008;85(2):247–255.
60. Oppmann B, et al. Novel p19 protein engages IL-12p40 to form a cytokine, IL-23, with biological activities similar as well as distinct from IL-12. *Immunity*. 2000;13(5):715–725.